

Cite this: *J. Mater. Chem. A*, 2019, 7, 18971

# p-Doping of organic hole transport layers in p–i–n perovskite solar cells: correlating open-circuit voltage and photoluminescence quenching†

Tian Du,<sup>‡</sup> Weidong Xu,<sup>‡</sup> Matyas Daboczi,<sup>‡</sup> Jinhyun Kim,<sup>b</sup> Shengda Xu,<sup>a</sup> Chieh-Ting Lin,<sup>‡</sup> Hongkyu Kang,<sup>cd</sup> Kwanghee Lee,<sup>d</sup> Martin J. Heeney,<sup>b</sup> Ji-Seon Kim,<sup>c</sup> James R. Durrant<sup>\*be</sup> and Martyn A. McLachlan<sup>‡\*a</sup>

Doping is a widely implemented strategy for enhancing the inherent electronic properties of charge transport layers in photovoltaic (PV) devices. Here, in direct contrast to existing understanding, we find that a reduction in p-doping of the organic hole transport layer (HTL) leads to substantial improvements in PV performance in planar p–i–n perovskite solar cells (PSCs), driven by improvements in open circuit voltage ( $V_{OC}$ ). Employing a range of transient and steady state characterisation tools, we find that the improvements of  $V_{OC}$  correlate with reduced surface recombination losses in less p-doped HTLs. A simple device model including screening of bulk electric fields in the perovskite layer is used to explain this observation. In particular, photoluminescence (PL) emission of complete solar cells shows that efficient performance is correlated to a high PL intensity at open circuit and a low PL intensity at short circuit. We conclude that desirable transport layers for p–i–n PSCs should be charge selective contacts with low doping densities.

Received 20th May 2019

Accepted 19th July 2019

DOI: 10.1039/c9ta03896e

rsc.li/materials-a

## Introduction

Perovskite solar cells (PSCs) with a p–i–n architecture are typified by a planar perovskite active layer (typically methylammonium lead halide, MAPI) sandwiched between a bottom p-type hole transport layer (HTL) and a top n-type electron transport layer (ETL). Such PSCs have drawn intensive research interest due not only to minimized current–voltage ( $J$ – $V$ ) hysteresis observed under operation<sup>1</sup> but also to their ease of fabrication.<sup>2</sup> For example, their low-temperature, solution-based processability is inherently compatible with large-volume manufacturing and enables their application in more complex device architectures *e.g.* tandem solar cells.<sup>3</sup> However, the attainable power conversion efficiencies (PCEs) of p–i–n devices are typically somewhat lower than those of their mesoporous or planar n–i–p analogues,<sup>4</sup> mainly because they typically exhibit a slightly lower open-circuit voltage ( $V_{OC}$ ).<sup>5</sup> Therefore it is of particular interest to determine the factors limiting the achievable  $V_{OC}$  of planar p–i–n PSCs.

Previous studies have demonstrated that the electronic band gap,<sup>6</sup> crystallinity<sup>7</sup> and microstructural defects<sup>8</sup> of the

photoactive perovskite layer are key factors determining device  $V_{OC}$  of PSCs. A further consideration are the recombination kinetics, where an increased rate of recombination is known to reduce  $V_{OC}$ .<sup>6</sup> Interestingly, when organic/polymeric charge transport layers are utilised, it has been demonstrated that PSC  $V_{OC}$  is insensitive to changes in either the highest occupied molecular orbital (HOMO) level of the HTLs employed<sup>9,10</sup> or to changes of the lowest unoccupied molecular orbital (LUMO) level of the ETL.<sup>11</sup> It has even been shown that some PSCs employing wide band gap perovskites yield  $V_{OC}$  values greater than the HTL-ETL energetic offset.<sup>12</sup> A widely recognized, but as yet relatively poorly understood issue in PSCs is surface recombination, in particular, for p–i–n devices, recombination that occurs at the interface between the perovskite active layer and the most widely used HTL, poly(3,4-ethylenedioxythiophene)-poly(styrenesulfonate) (PEDOT:PSS).<sup>13</sup> Several studies have identified this issue, and shown that modification or replacement of PEDOT:PSS can improve device  $V_{OC}$  and PCE.<sup>14–17</sup> Interestingly, in organic photovoltaics (OPVs) with analogous p–i–n architectures employing PEDOT:PSS as an HTL, surface recombination has

<sup>a</sup>Department of Materials and Centre for Plastic Electronics, Imperial College, London, SW7 2AZ, UK. E-mail: martyn.mclachlan@imperial.ac.uk

<sup>b</sup>Department of Chemistry and Centre for Plastic Electronics, Imperial College, London, SW7 2AZ, UK. E-mail: j.durrant@imperial.ac.uk

<sup>c</sup>Department of Physics and Centre for Plastic Electronics, Imperial College, London, SW7 2AZ, UK

<sup>d</sup>Research Institute for Solar and Sustainable Energies, Gwangju Institute of Science and Technology, Gwangju 61005, Republic of Korea

<sup>e</sup>SPECIFIC IKC, College of Engineering, Swansea University, SA2 7AX, UK

† Electronic supplementary information (ESI) available. See DOI: 10.1039/c9ta03896e

‡ These authors contributed equally to this work.

often been found to be less important as a loss pathway;<sup>18</sup> indeed in many cases, state-of-the-art OPV efficiencies have been reported using PEDOT:PSS.<sup>19</sup> The origin of the surface recombination losses in p-i-n perovskite solar cells, and how these may be reduced by selection of HTL, is thus currently poorly understood, and is the focus of the study reported herein.

The core function of a HTL is to selectively transfer photo-excited holes from the absorbing material to the external circuit, a process which in PSCs is often monitored by photoluminescence quenching (PLQ) measurements of the absorber interfaced with a HTL.<sup>20</sup> During such measurements, if high PLQ efficiency is observed when the absorber is interfaced with a HTL/ETL, this is frequently interpreted as an indication of effective charge transfer – and thus indicator of efficient photocurrent generation.<sup>21</sup> However such PLQ may also result from undesirable surface recombination losses, as widely reported for inorganic photovoltaic devices,<sup>22–25</sup> complicating the interpretation of such data. In addition, PL intensity in PSCs has been shown to be dependent on device measurement conditions *i.e.* typically higher at open circuit than short circuit,<sup>26</sup> and non-linearly dependent upon excitation intensity, a phenomenon ascribed to charge trapping and bimolecular recombination processes.<sup>27</sup> Indeed some studies have suggested that, due to the low electron–hole binding energy and relatively long carrier lifetimes reported for MAPI,<sup>28</sup> charge carriers accumulate primarily in the perovskite layer under open circuit conditions, and are not transferred to the HTL and ETL layers at open circuit.<sup>10</sup> The complexity of these factors has so far hindered our understanding of how significant charge transfer and extraction kinetics are to the PCE of PSCs, and how these compete with undesired recombination losses.

We focus here on the role of HTL in determining the  $V_{OC}$  and PCE of p-i-n, the so called inverted-architecture planar PSCs, specifically investigating the impact of p-doping of HTL on charge transfer and surface recombination. We have investigated a variety of HTLs in PSCs employing methylammonium lead iodide ( $\text{CH}_3\text{-NH}_3\text{PbI}_3$ , MAPI) as the common photoactive layer. Using poly(3,4-ethylenedioxythiophene)-poly(styrenesulfonate) (PEDOT:PSS) as our reference HTL we investigate key performance parameters when poly[bis(4-phenyl)(2,4,6-trimethylphenyl)amine] (PTAA) and poly[ $N,N'$ -bis(4-butylphenyl)- $N,N'$ -bis(phenyl)benzidine] (PTPD) are used as alternative HTLs. We demonstrate that variations in PL intensity observed between short and open circuit conditions are a powerful and relatively easy to obtain probe of surface recombination losses. From these studies, we conclude that reducing p-doping in HTLs is an effective strategy for reducing surface recombination losses in p-i-n perovskite solar cells and can result in enhanced device  $V_{OC}$  values and overall PCEs.

## Results

### Device performance based on different HTLs

P-i-n PSCs were prepared with a structure of glass/ITO/HTL/MAPI(500 nm)/PCBM(50 nm)/LiF(0.7 nm)/Ag (100 nm). Four HTLs, PEDOT:PSS (40 nm), PTAA (20 nm) and PTPD (20 nm) were deposited on indium-doped tin oxide (ITO) substrates, in

all cases the MAPI layers were fabricated with the same procedure.<sup>29</sup> The [6,6]-phenyl- $\text{C}_{61}$ -butyric acid methyl ester (PCBM) was deposited onto the MAPI layer as electron transport layer (ETL) and LiF/Ag bilayer was thermally evaporated on top of PCBM as cathode to complete the device. Prior to deposition of MAPI thin films, an ultrathin Poly [(9,9-bis(3'-( $N,N$ -dimethylamino)propyl)-2,7-fluorene)-*alt*-2,7-(9,9-dioctylfluorene)] (PFN) poly-electrolyte layer was spun onto PTPD and PTAA to reduce their surface hydrophobicity. Full device fabrication procedures and chemical structures (Fig. S1†) of the organic hole transport materials can be found in the ESI.†

Fig. 1a shows representative  $J$ - $V$  characteristics for devices prepared with the various HTLs measured under illumination and in the dark. The photovoltaic performance parameters based on 5 different pixels are also summarized in Table 1. The power conversion efficiency (PCE) of the PEDOT:PSS HTL device was determined to be  $13.5 \pm 0.2\%$ , which is consistent with existing literature,<sup>4</sup> when the alternative HTLs are employed PCE increases from  $17.6 \pm 0.3\%$  (PTAA) reaching  $19.6 \pm 0.2\%$  (PTPD). Analysis of the output characteristics makes it apparent that the observed overall performance improvements closely follow increases in open circuit voltage ( $V_{OC}$ ). It is noteworthy that none of the devices prepared exhibited appreciable  $J$ - $V$  hysteresis (Fig. S2†).

The external quantum efficiency (EQE) spectra of representative devices are shown in Fig. 1b, with a schematic illustration of the device structure shown in the inset. All devices show a comparable EQE onset at approximately 780 nm, but the device employing PEDOT:PSS has a couple of regions where the measured EQE is significantly less than the other materials. In Fig. 1c a flat-band energy diagram for these p-i-n devices is shown, in addition the HOMO levels of the HTLs, obtained by measuring their ionization potential through ambient pressure photoemission spectroscopy, are added (see Fig. S3 and Table S1†). Importantly, whilst there is some variation in the HOMO values between HTLs, there is no correlation between these values and the  $V_{OC}$  observed, consistent with existing literature.<sup>9</sup> The dashed lines in Fig. 1c indicate the equilibrium dark Fermi level of the HTLs measured with a Kelvin probe (Fig. S3 and Table S1†). The significance of this energetic difference between HOMO and Fermi level, labelled in the figure, will be discussed further below.

In order to exclude the possibility that the observed variations in  $V_{OC}$  are induced by structural or morphological variations in the MAPI layers on the various HTLs, we employed a range of complimentary characterisation techniques, namely X-ray diffraction (XRD) (Fig. S4a†); UV-vis absorption spectroscopy (Fig. S4b†) and scanning electron microscopy (SEM) (Fig. S5†). Analysis of the peak positions, intensities and full-widths at half-maximum (FWHM) of the XRD data (Table S2†) show no appreciable differences as the HTL is altered.<sup>7</sup> Similarly, the MAPI absorbance spectra show no significant differences as the HTLs change and the surface of the MAPI films, characterised by SEM, are comparable, with all showing a compact, coalesced structure with no observable variation in grain size nor the presence of pinholes. As such, we can conclude that the differences in device performance shown in

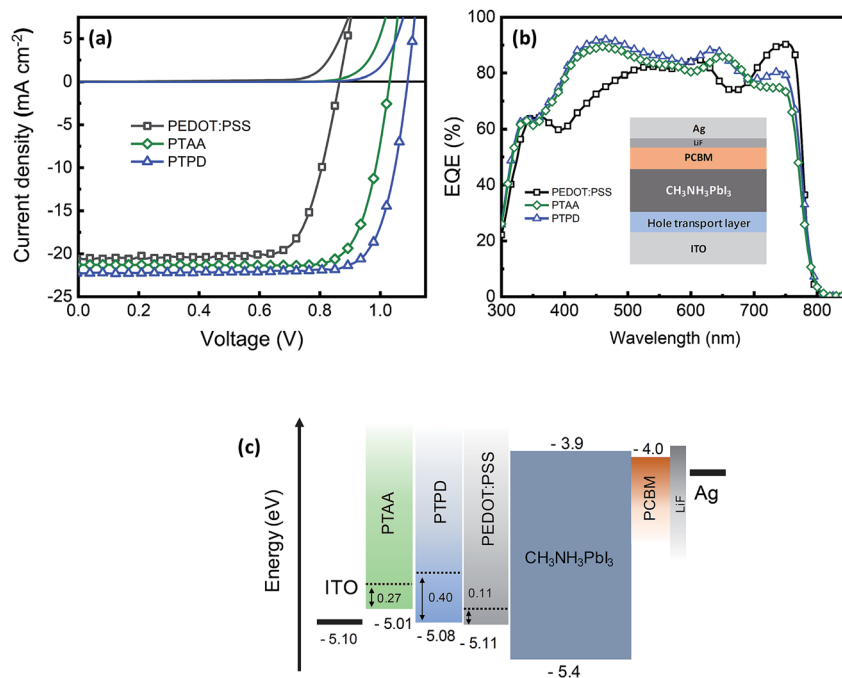


**Fig. 1** (a)  $J$ - $V$  curves of typical p-i-n perovskite solar cells based on PEDOT:PSS, PTAA and PTPD as HTLs, under AM1.5 1 Sun equivalent illumination at a scan rate of  $50 \text{ mV s}^{-1}$  in reverse bias. (b) External quantum efficiency (EQE) spectra of these devices. The inset figure shows a schematic drawing of device structure. (c) Schematic drawing of flat-band energy diagram of the solar cells, showing the highest occupied molecular orbital (HOMO) level, and equilibrium Fermi level (dashed lines) of these HTLs. The energetic differences between HOMO and Fermi level are calculated and labelled on the figure.

**Table 1** Measured photovoltaic parameters of p-i-n perovskite solar cells based on different HTLs, and PL quenching (PLQ<sub>BL</sub>) efficiencies measured for HTL/MAPI bilayer films relative to a bare MAPI film

	$J_{\text{SC}}$ (mA cm <sup>-2</sup> )	$V_{\text{OC}}$ (V)	FF	PCE (%)	PLQ <sub>BL</sub> efficiency (%)
PEDOT:PSS	$20.49 \pm 0.21$	$0.864 \pm 0.008$	$0.754 \pm 0.007$	$13.49 \pm 0.20$	98.2
PTAA	$21.38 \pm 0.35$	$1.033 \pm 0.003$	$0.795 \pm 0.007$	$17.58 \pm 0.31$	70.8
PTPD	$22.38 \pm 0.31$	$1.095 \pm 0.004$	$0.798 \pm 0.010$	$19.61 \pm 0.15$	32.9

Fig. 1 do not result from differences in the macroscopic properties of the MAPI layers in these devices.

### Photoluminescence quenching

We now consider photoluminescence quenching (PLQ) studies as a potential assay of hole transfer from MAPI to the HTLs. Fig. 2 shows PL emission spectra of a bare MAPI film and MAPI films in contact with the various HTLs. To ensure the PLQ measurements are relevant and comparable to the measurements made of operational devices, and in particular to avoid severe charge trapping effects observed within MAPI under low intensity irradiation conditions,<sup>20</sup> our PLQ measurements employed white light illumination at 1-Sun equivalent intensity. From these data, the bi-layer PLQ (PLQ<sub>BL</sub>) efficiency was estimated as the difference in emission intensity between a bare MAPI film and the various bilayers, listed in Table 1. From the table it is apparent that there is an inverse relationship between device PCE and PLQ<sub>BL</sub> efficiency – such that the bilayers

showing lower PLQ<sub>BL</sub> efficiency in the presence of HTL, in other words higher PL emission intensity in bilayers, yield the higher device PCE in complete devices. This observation is clearly counter to the widely used interpretation of PLQ<sub>BL</sub> as a measure of the efficiency of desired charge transfer to the transport layer, but is rather suggestive that for this sample series, higher PLQ<sub>BL</sub> may be indicative of enhanced surface recombination losses,<sup>24</sup> as we explore further below.

The bare MAPI and the MAPI/HTL bilayer films detailed in Fig. 2 were prepared using glass substrates and in the absence of a top electrode *i.e.* where there is no charge extraction to an external circuit and all photogenerated charges must ultimately recombine. Thus, our PL measurements were performed under conditions most equivalent to open circuit. We consider now the PL emission of the corresponding complete devices held under 1-Sun equivalent illumination at either open circuit or short circuit conditions, as shown in Fig. 3a–c. Under short circuit conditions, all devices showed similar, relatively low intensity photoluminescence (PL<sub>SC</sub>). This is indicative of

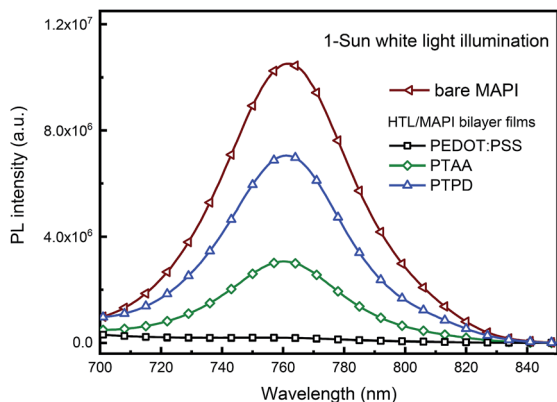


Fig. 2 PL emission of MAPI film and stacks of HTL/MAPI bilayer films under 1-Sun equivalent white-light illumination.

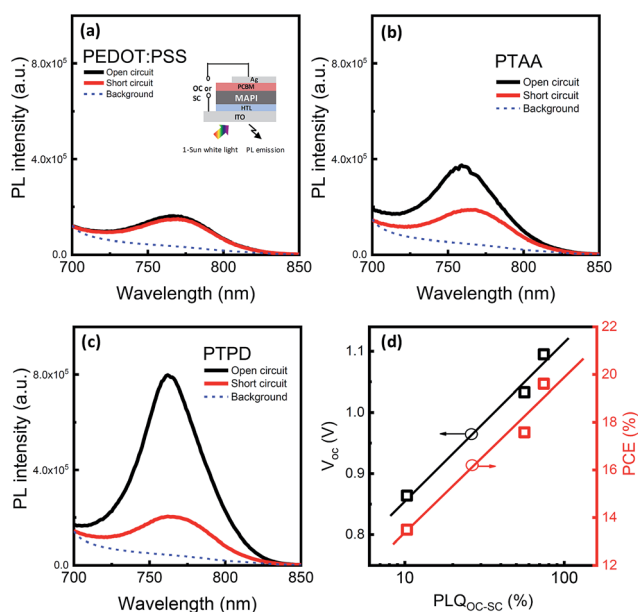


Fig. 3 (a–c) PL emission spectra of ITO/HTL/MAPI/PCBM/(LiF)Ag complete devices at short circuit and open circuit with PEDOT:PSS, PTAA and PTPD as HTL. The inset figure in (a) shows a schematic drawing of the measurements. (d) Correlation of  $V_{OC}$  and PCE versus OC-to-SC PL quenching efficiency ( $PLQ_{OC-SC}$ ) in complete devices.

efficient charge transfer to the ETL/HTL layers in these devices, most likely associated with efficient charge extraction to the external circuit under these conditions, suppressing radiative recombination in the absorber layer. The relative invariance of  $PL_{SC}$  between HTLs agrees with the relatively consistent  $J_{SC}$  values observed for these devices (Table 1). In contrast, the PL intensity measured at open circuit ( $PL_{OC}$ ) varies considerably between devices. In particular, we found that the relative intensity of  $PL_{OC}$  between these devices tracks the trend observed for the relative PL intensity of the bilayer films in Fig. 2. Whilst for efficient HTLs, *i.e.* PTPD, the PL intensity increases substantially between short and open circuit conditions, it is almost unchanged for the PEDOT:PSS device. To

quantify this effect, we determined the open-circuit-to-short-circuit (OC-to-SC) PL quenching efficiency ( $PLQ_{OC-SC}$ ) calculated as  $(PL_{OC} - PL_{SC})/PL_{OC}$ , describing the magnitude of the difference in PL emission intensity between open and short circuit. We note this quantification avoids the need to compare the absolute emission intensities between devices, which could also be influenced by the optical reflections of these devices. Fig. 3d plots the calculated values of device  $V_{OC}$  and PCE versus  $PLQ_{OC-SC}$ . A clear correlation is observed, with both PCE and  $V_{OC}$  correlated with an increase of  $PLQ_{OC-SC}$ . This implies that for the PSCs studied herein, enhanced device performance correlates with a high PL intensity at open circuit and low PL intensity at short circuit. This is consistent with general photovoltaic device physics,<sup>30</sup> with optical excitation of efficient devices expected to yield maximal radiative recombination at open circuit but efficient charge extraction at short circuit.<sup>31,32</sup> However, to the best of our knowledge, this behaviour has not previously been directly correlated with device efficiency for PSCs.

### The impact of HTL doping

Now we consider the origins of the observed variation in  $PLQ_{OC-SC}$  and  $V_{OC}$  between the HTLs studied here. As shown above neither the measured device  $V_{OC}$  nor PCE correlate with the HOMO levels of the HTLs, there is also no apparent correlation between the measured HTL Fermi level ( $E_F$ ) and the measured device performance metrics. We consider p-doping of the HTLs as a potential explanation for the observed behaviour. It is known that increased doping levels lead to greater HTL conductivity thus reduced the voltage losses due to electrical resistance.<sup>33,34</sup> We quantify p-doping for the various HTLs by calculating the energy difference between their HOMO and  $E_F$  values, Fig. 1c. This energy difference, denoted as  $E_F - E_{HOMO}$ , indicates the relative p-type doping levels to be PEDOT:PSS > PTAA > PTPD. Utilising these data, we plot the measured  $PLQ_{BL}$ ,  $PLQ_{OC-SC}$ , device  $V_{OC}$  and PCE versus measured  $E_F - E_{HOMO}$  (Fig. 4a–b). It is clear from Fig. 4a that as p-doping of HTL increases, there is a decrease in  $PLQ_{BL}$  measured in the presence of the HTLs, and an increase in  $PLQ_{OC-SC}$  in complete devices, suggesting that increased p-doping of our HTLs quenches PL emission at OC. This correlates with the trend shown in Fig. 4b showing that both increased  $V_{OC}$  and PCE derives from a reduction in HTL p-doping. It is thus evident that the devices with the highest measured  $V_{OC}$ , and therefore PCE, are those that employ least p-doped HTLs.

### Evidence of surface recombination

When combined, these data support the suggestion that the observed variations in device performance are not related to shift of HOMO levels but most likely originate from differences in surface recombination losses, and specifically that these surface recombination losses are primarily determined by the extent of p-doping of the HTL layer. To probe further the recombination losses in our device series we consider now more in-depth analysis of device optoelectronic performance.

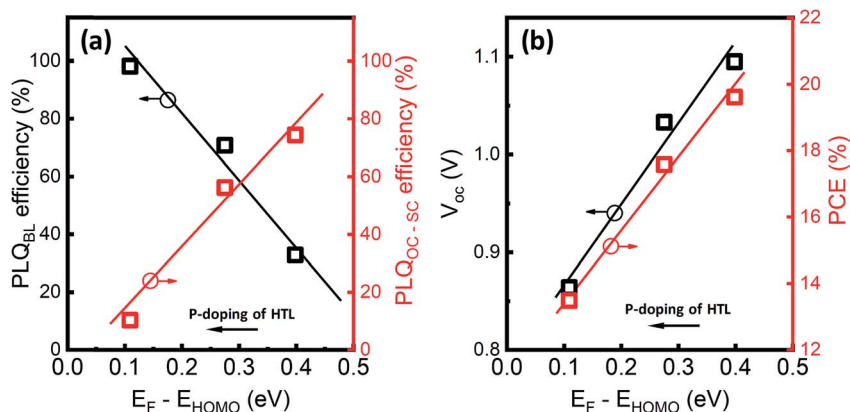


Fig. 4 (a) Correlation of photoluminescence quenching efficiency in HTL/MAPI bilayer films (PLQ<sub>BL</sub>) and in complete devices between open circuit and short circuit (PLQ<sub>OC-sc</sub>), with the p-doping level of HTL that is estimated by the difference of HOMO and Fermi level,  $E_F - E_{\text{HOMO}}$ . (b) Correlation of device  $V_{\text{OC}}$  and PCE with the  $E_F - E_{\text{HOMO}}$  of HTL.

One widely used assay of such recombination losses is to measure the evolution of  $V_{\text{OC}}$  with light intensity to derive an ideality factor  $n_{\text{id}}$  from the slope of  $V_{\text{OC}}$ -light intensity relationship:  $n_{\text{id}} = \frac{q}{k_{\text{B}}T} \frac{\delta V_{\text{OC}}}{\delta \ln(I)}$ , where  $k_{\text{B}}T$  is the thermal energy,  $I$  the light intensity and  $q$  the unit charge. Fig. 5a shows the semi-logarithmic plot of steady state  $V_{\text{OC}}$  versus light intensity, and the  $n_{\text{id}}$  values obtained by fitting the plot between 0.04–4 Suns. The most efficient devices *i.e.* those with higher  $V_{\text{OC}}$  and PTPD

and PTAA as HTLs, both show rather large values of  $n_{\text{id}}$ , 1.79 and 1.70 respectively. In contrast, devices with lower  $V_{\text{OC}}$ , as seen with PEDOT:PSS HTLs, exhibited lower  $n_{\text{id}}$  of 1.12. A lower  $n_{\text{id}}$  in combination with lower device  $V_{\text{OC}}$  is typically attributed to the devices limited by monomolecular surface recombination at the contacts,<sup>16,35,36,37</sup> resulting in less steep increase of  $V_{\text{OC}}$  with light intensity in the semi-logarithmic plot. Interestingly, devices with high  $V_{\text{OC}}$  and high PCE exhibiting  $n_{\text{id}}$  values close to 2 have also been reported for efficient n-i-p, conventional

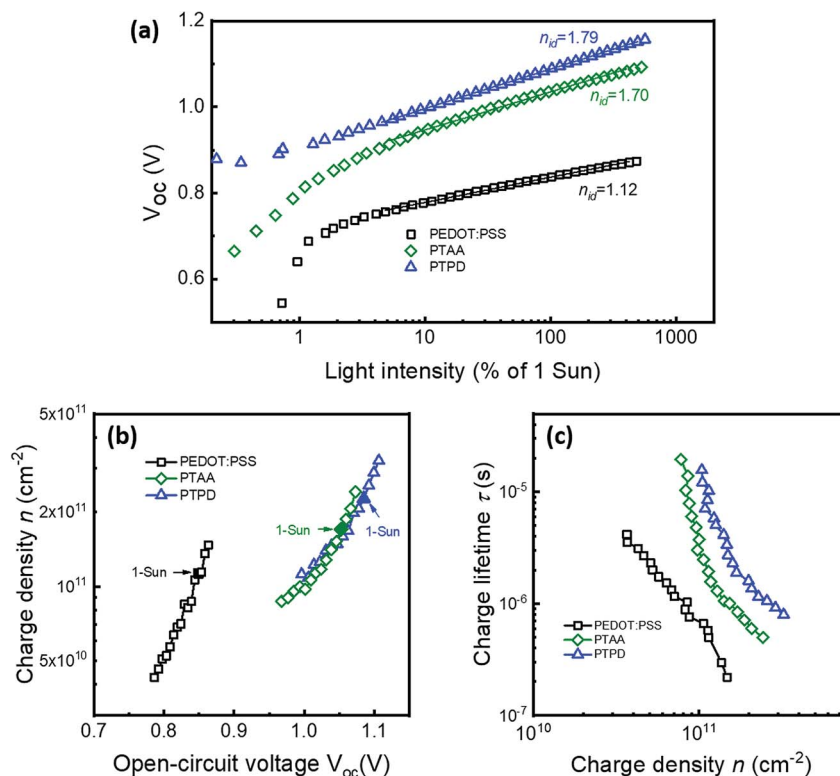


Fig. 5 (a) Evolution of device  $V_{\text{OC}}$  as a function of light intensity, and the light ideality factor  $n_{\text{id}}$  derived from fitting the plot between 0.04–4 Suns. (b) Charge carrier density  $n$  as a function of  $V_{\text{OC}}$  in the solar cells with various HTLs. The solid symbol corresponding to approximate 1-Sun condition. (c) Charge recombination lifetime  $\tau$  derived from transient photovoltage (TPV) decay as a function of  $n$ .

PSC's,<sup>35</sup> indicative of higher order losses such as bimolecular recombination. These data thus are consistent with non-radiative recombination at open circuit in PEDOT:PSS cells being related to the presence of monomolecular recombination at HTL/MAPI interface, often referred to as surface recombination.

To support these hypotheses, and correlate the observed variation in  $V_{OC}$  to modulations in the p-doping of the HTL influencing surface recombination at the MAPI/HTL interface, we carried out additional transient optoelectronic measurements at varying illumination intensities to determine accumulated charge densities and charge recombination lifetimes at open circuit as a function of device  $V_{OC}$ . A description of these techniques is given in the experimental section and Fig. S6–S8,† and can be found in detail elsewhere.<sup>6,38</sup> For all devices, these analyses correctly predicted device  $V_{OC}$  to within  $\pm 6$  mV within the probed light levels, confirming the validity of these analyses (Fig. S9†). Fig. 5b plots the excess (photo-generated) charge density ( $n$ ) in these devices as a function of  $V_{OC}$ , in which all devices show an approximately exponential increase of  $n$  with  $V_{OC}$ , assigned to charge “stored” in the electronic states of MAPI and/or contact layers. The overall charge recombination kinetics of the complete devices can be quantified by the lifetime of charge carriers ( $\tau$ ) derived from TPV decays, plotted in Fig. 5c as a function of charge density. The slope of the  $n$  vs.  $V_{OC}$  plots for all of the HTLs investigated are similar (Fig. 5b) suggesting that these devices are dominated by charge accumulation in the MAPI layer. This is consistent with our recent work employing PEDOT:PSS as an HTL in p–i–n devices, where we found that at very low light intensities photogenerated charge accumulated primarily on the device contacts and at higher intensities, as employed for the data in Fig. 5b and c, that charge primarily accumulated within the MAPI layer.<sup>6</sup> It is striking that the PEDOT:PSS device data in Fig. 5b shows equivalent accumulated charge densities at much lower measured  $V_{OC}$  values than the devices with a lesser degree of p-doping. As the accumulated charge density is a measure of the active layer quasi-Fermi level splitting, this observation implies that when employing PEDOT:PSS as the HTL, the externally measured  $V_{OC}$  is substantially ( $\sim 150$  mV) less than active layer quasi-Fermi level splitting. We have previously obtained analogous data in organic solar cells as a function of metal-oxide HTL processing conditions, and have shown, with the aid of device modelling, that such a reduction in  $V_{OC}$  relative to active layer quasi-Fermi level splitting is expected in the presence of surface recombination losses.<sup>36</sup> The presence of surface recombination losses is further supported by Fig. 5c, which shows that increased HTL p-doping is correlated with faster recombination kinetics for matched densities of accumulated charge. This trend was also observed for organic solar cells with increased surface recombination losses.<sup>36</sup> As a result of these slower recombination kinetics, devices with suppressed surface recombination can “store” more photo-excited charge within the active layer under 1 Sun (these conditions are marked as solid symbols in Fig. 5b). This gives rise to an additional increase of  $V_{OC}$  by about 50–85 mV for the less p-doped HTL's compared to PEDOT:PSS. The approximate 1-Sun accumulated charge densities are PTPD ( $2.3 \times 10^{11} \text{ cm}^{-2}$ ) >

PTAA ( $1.7 \times 10^{11} \text{ cm}^{-2}$ ) > PEDOT:PSS ( $1.1 \times 10^{11} \text{ cm}^{-2}$ ). These correlate with the order of their  $PL_{OC}$  intensities, consistent with higher accumulated charge densities resulting from suppressed non-radiative, in this case surface, recombination and thus resulting in enhanced radiative recombination and therefore PL. In summary, our ideality factor and transient optoelectronic measurements all support enhanced surface recombination losses with more doped HTLs, resulting in devices with reduced  $V_{OC}$ .

## Discussion

We have demonstrated the significance of p-doping in the HTL of p–i–n PSCs, specifically that a reduction in p-doping results in significant improvements in device  $V_{OC}$  and PCE. By employing a range of complimentary techniques, including photoluminescence quenching, photoemission spectroscopy and kelvin probe analyses, device ideality factor and measurements of charge carrier densities and lifetimes at open circuit, we conclude that the reduction in device  $V_{OC}$  observed in more p-doped HTLs results from enhanced surface recombination losses. In particular we find that measurement of the open-circuit-to-short-circuit (OC-to-SC) PL quenching efficiency is an effective assay of such surface recombination losses, with high device performance correlating with a high PL intensity at open circuit (where charges are primarily confined to, and recombine in, the photoactive layer) and a low PL intensity at short circuit (where charges are efficiently extracted to the external circuit). Therefore we conclude that minimisation of HTL doping is a key consideration for the optimization of the performance of planar p–i–n PSCs.

The enhanced surface recombination losses for p-doped HTL layers implies this recombination is associated with the dark charge present in these layers, rather than photoinjected charge. Typical carrier densities in PEDOT:PSS thin films are approximately  $2 \times 10^{20} \text{ cm}^{-3}$ ,<sup>39</sup> corresponding to  $8 \times 10^{14} \text{ cm}^{-2}$  for the 40 nm film deposited in our devices. This is approximately 3-orders of magnitude greater than the photogenerated charge density in PEDOT:PSS devices under 1-Sun illumination at open circuit ( $1.1 \times 10^{11} \text{ cm}^{-2}$ ). Thus it can be concluded that when employing PEDOT:PSS, the density of dark charge carriers in the HTL available to undergo recombination processes is far higher than the density of photogenerated carriers. In this context, the enhanced surface recombination with greater HTL p-doping can be understood in terms of a loss of selectivity of the HTL due to the high dark carrier density, enabling not only hole but also electron transfer to the HTL layer, resulting in a net loss of photocarriers. It is apparent that this origin of surface recombination is distinct from that often observed in other inorganic solar cells such as silicon or cadmium telluride, where surface recombination is often reported to be mediated by dangling bonds at surfaces or grain boundaries, resulting in trap mediated surface recombination.<sup>30</sup> We note the mechanism of surface recombination we find here also differs from that often discussed in n–i–p PSC's employing  $\text{TiO}_2$  as ETL, where trap states at the  $\text{TiO}_2$ /perovskite interface have been reported to mediate surface recombination losses<sup>40,41</sup> and has

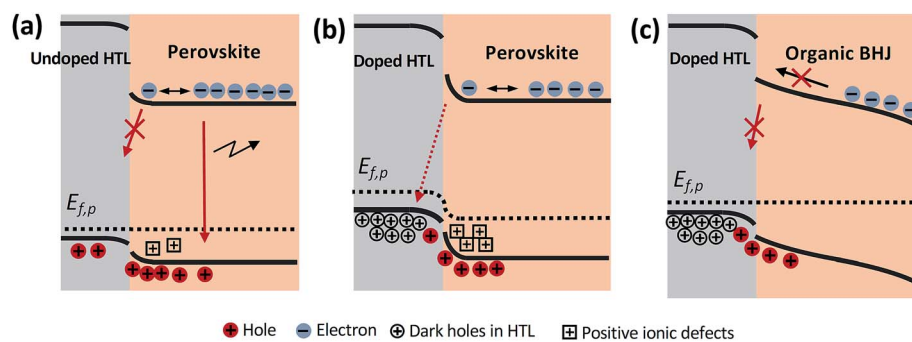


Fig. 6 Schematic drawing of open circuit band diagram and charge accumulation/combination in the HTL interface in a p–i–n perovskite solar cells with (a) an undoped HTL and (b) a doped HTL, and (c) in a typical organic bulk heterojunction (BHJ) solar cell with doped HTL.

also been associated with the observation of  $J$ - $V$  hysteresis in the n–i–p devices,<sup>42,43</sup> which is otherwise absent in the p–i–n devices studied in this work.

In contrast to the conclusions we find here for planar p–i–n PSCs, highly doped PEDOT:PSS is widely used in OPVs<sup>19</sup> and in hybrid silicon/PEDOT:PSS solar cells<sup>44</sup> yielding excellent device performance. In such devices, efficient performance has also been observed with other doped HTLs.<sup>34,45</sup> It is therefore interesting to consider why PSCs are more susceptible to efficiency losses associated with surface recombination with doped HTLs than OPVs. We describe the difference in recombination mechanisms in the schematic shown in Fig. 6a–c. Fig. 6c illustrates a typical energy level diagram for an OPV at open circuit. In this case, the built-in potential drops across the photoactive layer, forming an electric field that drives holes to the HTL and electrons to the ETL. As such, this built in field suppresses surface recombination losses at the HTL/organic interface, even when this HTL is doped, as it drives electrons away from this interface.<sup>46</sup> In contrast, in PSCs, screening effects caused by the diffusion of ionic defects in the MAPI layer<sup>47</sup> confine the potential drop in the MAPI layer to a thin space charge layer near the device interfaces, with the MAPI bulk being field-free,<sup>48</sup> as shown in Fig. 6a–b. Such field screening allows for considerable electron diffusion towards the HTL/perovskite interface, and therefore the potential for photo-generated electrons to recombine with holes in the HTL, resulting in surface recombination (Fig. 6b). This provides a rationale for our observation herein that employing an undoped, selective HTL is more critical for perovskite solar cells than for analogous organic solar cells.

Our analyses indicate that non-selective, heavily doped contacts, widely used in OPVs, are not desirable for PSCs. As lower doping levels reduce conductivity, the thickness of the HTL must be controlled to minimize series resistance losses. For example, for the devices studied in our work, increasing the thickness of the PTPD layer above 20 nm significantly reduced device FF and  $J_{SC}$ , whereas thickness variations of the PEDOT:PSS and doped PTAA layers did not cause appreciable degradation of device performance (Fig. S10†). The lower conductivity of the less p-doped HTLs can also be a potential problem for n–i–p PSCs where PTAA layer thicknesses much thicker than those explored herein can be required to effectively

cover the perovskite active layer – hence in such circumstances doping of PTAA is typically required to improve conductivity. Interestingly extreme doping of PTAA with lithium salts in such devices has been reported to result in a  $> 200$  mV loss in  $V_{OC}$ ,<sup>49</sup> a case we consider to be analogous to our results.

Our observation that the best performing p–i–n PSC studied here exhibits the highest device PL efficiency, when measured under open circuit conditions, is comparable to observations in inorganic solar cells.<sup>22–24</sup> Under open circuit conditions, all charge must recombine in the device; a high PL efficiency measured under these conditions implies a suppression of undesirable non-radiative recombination losses, and thus an enhancement of bulk, radiative recombination. This observation is agreement with the trend in PL studies of neat perovskite films and with device electroluminescence studies, where in both cases higher emission intensities correlated with higher photovoltaic device performance.<sup>7,14,50</sup> Our observations are also consistent with a recent study by Wolff *et al.*,<sup>11</sup> which showed that introducing a charge blocking layer at the perovskite/ETL interface resulted in enhanced bulk recombination relative to surface recombination, and yielded a higher  $V_{OC}$ . We conclude that by suppressing surface recombination, and thus confining recombination to the absorber layer, higher device  $V_{OC}$  and PCE can be achieved. As such, minimizing bulk non-radiative recombination losses within the MAPI layer, either by passivating bulk defects<sup>51</sup> or optimizing the perovskite composition,<sup>52</sup> as well as minimising recombination at the MAPI/ETL interface, should lead to further improvements in device performance.

## Author contributions

T. D. fabricated the solar cells, performed the photovoltaic and optoelectronic measurements. W. X., T. D. and J. K. carried out photoluminescence spectroscopic measurements. M. D. measured the HOMO levels and work functions of the HTLs. S. X. obtained the SEM images and absorption measurement. C. L. contributed to device fabrication and EQE measurement. K. L., H. K., M. J. H., J.-S. K., M. A. M. and J. R. D all contributed to project planning and discussion. T. D. prepared the original draft, which was revised by W. X., J. R. D and M. A. M. All authors contributed to the manuscript preparation. T. D. and W. X. contributed equally to this work.

## Conflicts of interest

The authors declare no competing financial interests.

## Acknowledgements

The authors acknowledge funding from Stephen and Ana Hui Fellowship (Imperial College London), China Scholarship Council and Welsh government Sêr Cymru Solar programme. This work was supported by GIST Research Institute (GRI) grant funded by the GIST in 2019; the Global Research Laboratory Program of the National Research Foundation (NRF) funded by the Ministry of Science, ICT & Future Planning (NRF-2017K1A1A2013153); the GIST-ICL International Collaboration R&D Centre. Additionally, we acknowledge the EPSRC Centre for Doctoral Training in Plastic Electronic Materials EP/L016702/1 for continued student support and training. The authors are grateful to Professor Iain McCulloch (ICL/KAUST) for useful discussions on the HTLs during peer-review.

## References

- 1 J. H. Heo, H. J. Han, D. Kim, T. K. Ahn and S. H. Im, *Energy Environ. Sci.*, 2015, **8**, 1602–1608.
- 2 J. You, Z. Hong, Y. M. Yang, Q. Chen, M. Cai, T.-B. Song, C.-C. Chen, S. Lu, Y. Liu and H. Zhou, 2014.
- 3 K. A. Bush, A. F. Palmstrom, Z. J. Yu, M. Bocard, R. Checharoen, J. P. Mailoa, D. P. McMeekin, R. L. Z. Hoye, C. D. Bailie, T. Leijtens, I. M. Peters, M. C. Minichetti, N. Rolston, R. Prasanna, S. Sofia, D. Harwood, W. Ma, F. Moghadam, H. J. Snaith, T. Buonassisi, Z. C. Holman, S. F. Bent and M. D. McGehee, *Nat. Energy*, 2017, **2**, 1–7.
- 4 L. Meng, J. You, T. F. Guo and Y. Yang, *Acc. Chem. Res.*, 2016, **49**, 155–165.
- 5 W. Tress, *Adv. Energy Mater.*, 2017, **7**, 1602358.
- 6 S. Wheeler, D. Bryant, J. Troughton, T. Kirchartz, T. M. Watson, J. Nelson and J. R. Durrant, *J. Phys. Chem. C*, 2017, **121**, 13496–13506.
- 7 T. Du, J. Kim, J. Ngiam, S. Xu, P. R. F. Barnes, J. R. Durrant and M. A. McLachlan, *Adv. Funct. Mater.*, 2018, **2**, 1801808.
- 8 T. Du, C. H. Burgess, C.-T. Lin, F. Eisner, J. Kim, S. Xu, H. Kang, J. R. Durrant and M. A. McLachlan, *Adv. Funct. Mater.*, 2018, **28**, 1803943.
- 9 R. A. Belisle, P. Jain, R. Prasanna, T. Leijtens and M. D. McGehee, *ACS Energy Lett.*, 2016, **1**, 556–560.
- 10 J. Jiménez-López, W. Cambarau, L. Cabau and E. Palomares, *Sci. Rep.*, 2017, **7**, 6101.
- 11 C. M. Wolff, F. Zu, A. Paulke, L. P. Toro, N. Koch and D. Neher, *Adv. Mater.*, 2017, **29**, 1–8.
- 12 M. I. Dar, M. Franckevičius, N. Arora, K. Redekas, M. Vengris, V. Gulbinas, S. M. Zakeeruddin and M. Grätzel, *Chem. Phys. Lett.*, 2017, **683**, 211–215.
- 13 K. G. Lim, H. B. Kim, J. Jeong, H. Kim, J. Y. Kim and T. W. Lee, *Adv. Mater.*, 2014, **26**, 6461–6466.
- 14 D. B. Khadka, Y. Shirai, M. Yanagida, J. W. Ryan and K. Miyano, *J. Mater. Chem. C*, 2017, **5**, 8819–8827.
- 15 C. Bi, Q. Wang, Y. Shao, Y. Yuan, Z. Xiao and J. Huang, *Nat. Commun.*, 2015, **6**, 7747.
- 16 K. Tvingstedt, L. Gil-Escrig, C. Momblona, P. Rieder, D. Kiermasch, M. Sessolo, A. Baumann, H. J. Bolink and V. Dyakonov, *ACS Energy Lett.*, 2017, **2**, 424–430.
- 17 N. Wijeyasinghe, A. Regoutz, F. Eisner, T. Du, L. Tsetseris, Y. H. Lin, H. Faber, P. Pattanasattayavong, J. Li, F. Yan, M. A. McLachlan, D. J. Payne, M. Heeney and T. D. Anthopoulos, *Adv. Funct. Mater.*, 2017, **27**, 1701818.
- 18 B. Maennig, J. Drechsel, D. Gebeyehu, P. Simon, F. Kozłowski, A. Werner, F. Li, S. Grundmann, S. Sonntag, M. Koch, K. Leo, M. Pfeiffer, H. Hoppe, D. Meissner, N. S. Sariciftci, I. Riedel, V. Dyakonov and J. Parisi, *Appl. Phys. A*, 2004, **79**, 1–14.
- 19 Z. He, C. Zhong, S. Su, M. Xu, H. Wu and Y. Cao, *Nat. Photonics*, 2012, **6**, 593–597.
- 20 J. Kim, R. Godin, S. D. Dimitrov, T. Du, D. Bryant, M. A. McLachlan and J. R. Durrant, *Adv. Energy Mater.*, 2018, **35**, 1802474.
- 21 H. Cha, J. Wu, A. Wadsworth, J. Nagitta, S. Limbu, S. Pont, Z. Li, J. Searle, M. F. Wyatt, D. Baran, J. S. Kim, I. McCulloch and J. R. Durrant, *Adv. Mater.*, 2017, **29**, 1–8.
- 22 M. J. Yang, M. Yamaguchi, T. Takamoto, E. Ikeda, H. Kurita and M. Ohmori, *Sol. Energy Mater. Sol. Cells*, 1997, **45**, 331–339.
- 23 S. Shirakata and T. Nakada, *Thin Solid Films*, 2007, **515**, 6151–6154.
- 24 W. K. Metzger, D. Albin, D. Levi, P. Sheldon, X. Li, B. M. Keyes and R. K. Ahrenkiel, *J. Appl. Phys.*, 2003, **94**, 3549–3555.
- 25 W. K. Metzger, I. L. Repins, M. Romero, P. Dippo, M. Contreras, R. Noufi and D. Levi, *Thin Solid Films*, 2009, **517**, 2360–2364.
- 26 K. Tvingstedt, O. Malinkiewicz, A. Baumann, C. Deibel, H. J. Snaith, V. Dyakonov and H. J. Bolink, *Sci. Rep.*, 2014, **4**, 1–7.
- 27 X. Wen, Y. Feng, S. Huang, F. Huang, Y. Cheng, M. Green and A. Ho-baillie, *J. Mater. Chem. C*, 2015, **4**, 793–800.
- 28 C. Wehrenfennig, G. E. Eperon, M. B. Johnston, H. J. Snaith and L. M. Herz, *Adv. Mater.*, 2014, **26**, 1584–1589.
- 29 J. LeeH. Kang, G. Kim, H. Back, J. Kim, S. Hong, B. Park, E. Lee, K. Lee, 2017, **29**, 1606363.
- 30 J. Nelson, *The physics of solar cells*, World Scientific, 2003, vol. 57.
- 31 E. Yablonovitch, *Science*, 2016, **351**, 1401.
- 32 D. Bryant, N. Aristidou, S. Pont, I. Sanchez-Molina, T. Chotchunangatchaval, S. Wheeler, J. R. Durrant and S. A. Haque, *Energy Environ. Sci.*, 2016, **9**, 1655–1660.
- 33 J. Burschka, A. Dualeh, F. Kessler, E. Baranoff, N. L. Cevy-Ha, C. Yi, M. K. Nazeeruddin and M. Grätzel, *J. Am. Chem. Soc.*, 2011, **133**, 18042–18045.
- 34 M. D. Irwin, D. B. Buchholz, A. W. Hains, R. P. H. Chang and T. J. Marks, *Proc. Natl. Acad. Sci. U.S.A.*, 2008, **105**, 2783–2787.
- 35 W. Tress, M. Yavari, K. Domanski, P. K. Yadav, B. Niesen, J.-P. Correa-Baena, A. Hagfeldt and M. Grätzel, *Energy Environ. Sci.*, 2017, **11**, 151–165.

- 36 S. Wheeler, F. Deledalle, N. Tokmoldin, T. Kirchartz, J. Nelson and J. R. Durrant, *Phys. Rev. Appl.*, 2015, **4**, 024020.
- 37 T. Kirchartz and J. Nelson, *Phys. Rev. B: Condens. Matter Mater. Phys.*, 2012, **86**, 1–12.
- 38 B. C. O'Regan, P. R. F. Barnes, X. Li, C. Law, E. Palomares and J. M. Marin-Beloqui, *J. Am. Chem. Soc.*, 2015, **137**, 5087–5099.
- 39 M. Yamashita, C. Otani, H. Okuzaki and M. Shimizu, *2011 30th URSI Gen. Assem. Sci. Symp. URSIGASS 2011*, 2011, vol. 1, pp. 3–6.
- 40 F. Zhang, W. Ma, H. Guo, Y. Zhao, X. Shan, K. Jin, H. Tian, Q. Zhao, D. Yu, X. Lu, G. Lu and S. Meng, *Chem. Mater.*, 2016, **28**, 802–812.
- 41 T. Leijtens, G. E. Eperon, S. Pathak, A. Abate, M. M. Lee and H. J. Snaith, *Nat. Commun.*, 2013, **4**, 2885.
- 42 T. Du, C. H. Burgess, J. Kim, J. Zhang, J. R. Durrant and M. A. McLachlan, *Sustain. Energy Fuels*, 2017, **1**, 119–126.
- 43 S. Van Reenen, M. Kemerink and H. J. Snaith, *J. Phys. Chem. Lett.*, 2015, **6**, 3808–3814.
- 44 S. Jäckle, M. Mattiza, M. Liebhaber, G. Brönstrup, M. Rommel, K. Lips and S. Christiansen, *Sci. Rep.*, 2015, **5**, 1–12.
- 45 N. Wijeyasinghe, F. Eisner, L. Tsetseris, Y. H. Lin, A. Seitkhan, J. Li, F. Yan, O. Solomeshch, N. Tessler, P. Patsalas and T. D. Anthopoulos, *Adv. Funct. Mater.*, 2018, **28**, 1–14.
- 46 D. Credgington, F. C. Jamieson, B. Walker, T. Q. Nguyen and J. R. Durrant, *Adv. Mater.*, 2012, **24**, 2135–2141.
- 47 R. A. Belisle, W. H. Nguyen, A. R. Bowring, P. Calado, X. Li, S. J. C. Irvine, M. D. McGehee, P. R. F. Barnes and B. C. O'Regan, *Energy Environ. Sci.*, 2017, **10**, 192–204.
- 48 P. Calado, A. M. Telford, D. Bryant, X. Li, J. Nelson, B. C. O'Regan and P. R. F. Barnes, *Nat. Commun.*, 2016, **7**, 13831.
- 49 J.-P. Correa-Baena, W. Tress, K. Domanski, E. H. Anaraki, S.-H. Turren-Cruz, B. Roose, P. P. Boix, M. Grätzel, M. Saliba, A. Abate and A. Hagfeldt, *Energy Environ. Sci.*, 2017, **10**, 1207–1212.
- 50 Y. Hou, W. Chen, D. Baran, T. Stubhan, N. A. Luechinger, B. Hartmeier, M. Richter, J. Min, S. Chen, C. O. R. Quiroz, N. Li, H. Zhang, T. Heumueller, G. J. Matt, A. Osvet, K. Forberich, Z. G. Zhang, Y. Li, B. Winter, P. Schweizer, E. Spiecker and C. J. Brabec, *Adv. Mater.*, 2016, 5112–5120.
- 51 X. Zheng, B. Chen, J. Dai, Y. Fang, Y. Bai, Y. Lin, H. Wei, X. C. Zeng and J. Huang, *Nat. Energy*, 2017, **2**, 17102.
- 52 M. Saliba, T. Matsui, J.-Y. Seo, K. Domanski, J.-P. Correa-Baena, M. K. Nazeeruddin, S. M. Zakeeruddin, W. Tress, A. Abate, A. Hagfeldt and M. Grätzel, *Energy Environ. Sci.*, 2016, **9**, 1989–1997.